PRELIMINARY VALIDATION OF SMOS PRODUCTS (LEVELS 3 AND 4)

J. Gourrion[1,2], J. Ballabrera[1,3], A.L. Aretxabaleta[1,2], A. Turiel[1,2], B. Mourre[4], S. Kalaroni[1,2], and N. Hoareau[1,2]

[1]SMOS Barcelona Expert Centre on Radiometric Calibration and Ocean salinity, Spain
[2]Institut de Ciències del Mar CSIC, Barcelona, Spain; [3]Unitat de Tecnologia Marina CSIC, Barcelona, Spain
[4]NATO Underwater Research Centre, La Spezia, Italy

ABSTRACT

With the advent of ESA's SMOS Mission, we have the opportunity for the first time of measuring Sea Surface Salinity (SSS) from the space and at a synoptic scale. However, the MIRAS instrument onboard SMOS is a new concept of instrument, and the adjustment and calibration of this interferometric radiometer poses great challenges. In this paper, we show the present status of Level 3 and 4 salinity maps, which are supposed to give accurate climatological descriptions of SSS, describing the attained accuracy and analyzing the geophysical consistence of those maps. A discussion on future improvements is also issued.

Index Terms— SMOS, Sea Surface Salinity, match-up, Level 3 and 4.

1. INTRODUCTION

The Soil Moisture and Ocean Salinity mission (SMOS) from the European Space Agency, launched in November 2009, has initiated the era of satellite-based salinity observations. However, because of low radiometric sensitivity to Sea Surface Salinity (SSS), numerous geophysical contamination sources and the retrieval complexity, salinity products will have a low signal-to-noise ratio at Level 2 [1].

As projected in the mission design, averaging data in space and time is expected to allow a reduction of the observational error down to mission requirements (0.1 psu) at Level 3 (global maps with regular distribution) [2].

Robust, geophysical consistency is expected to be reached at Level 4, when the SMOS salinity data are combined with data from other sources as, for example, satellite sea surface temperature, surface winds, estimates of evaporation and precipitation, and even remotely-sensed ocean color. Present day calibration and contamination issues completely preclude the obtaining of a meaningful Level 4 product. We will concentrate our discussion on the issues detected at Level 3, with a brief discussion on future directions for Level 4.

This work has been funded by the Spanish Ministry of Education and Science through research grants ESP2005-06823-C05-01 and ESP2007-65667-C04

The paper is structured as follows: Section 2 briefly describes the process for the estimation of SSS from SMOS raw measurements up to Level 3. Then, in Section 3 we present the results of the comparison of one Level 3 map with the corresponding World Ocean Atlas (WOA) climatological map. The same exercise is repeated in Section 4 but using in-situ measurements by ARGO floats. Then, the congruency of geophysical structures in SSS maps is analyzed with advanced signal processing tools in Section 5. Section 6 is devoted to summarize the work and present the conclusions.

2. SALINITY RETRIEVAL

For this study, the L1B product derived from ascending orbits in the period extending from March 10 to March 15, 2010 is used. These products have been downloaded from the SMOS Data Processing Ground Segment (DPGS), corresponding the version 3.3.0 of the Level 1 Operational Processor. The Brightness Temperature (T_B) in the antenna frame has been derived, and the images geolocated. That specific week of data was acquired under the Full-polarization operation mode, the final nominal operation mode of MIRAS. In order to derive the associated SSS, we have used a geophysical model that includes auxiliary information from the other relevant geophysical variables (SST, wind) provided by the European Center for Medium-range Weather Forecast (ECMWF).

2.1. Data selection:

During the course of the mission, it has been reported that land contamination can affect large areas, far from coast, due to some unsolved problems in the reconstruction algorithm. For that reason and, to obtain a product as free of land contamination as possible, snapshots with more than 10 points (over 4096 points) over land have been discarded. A further filtering is applied by discarding those snapshots for which any point displays a discrepancy (SMOS T_B minus modeled T_B) larger than 20K. This is expected to minimize Radio Frequency Interference (RFI) impacts.

2.2. SSS inversion scheme

For each point in one valid snapshot, a cursory SSS inversion scheme is applied to each individual X- and Y-pol T_B. The auxiliary wind speed and SST data are assumed to be ground truth. Although these parameters come from a numerical model, their relative errors are considerable less than those of the present configuration of the instrument, and so their erros may be neglected in a first approximation. The SSS climatology obtained from WOA is used to derive both the first-guess of T_B and its gradient with respect to SSS. The retrieved SSS is the linear correction to climatology, and is proportional to the difference between the measured and the modelled T_B.

2.3. L3 product

We have created two Level 3 products, one for X polarization and one for the Y one, by combining all the valid L2 SSS maps from the previous section. The L3 maps are binned weighted averages of the L2 fields onto a regular cylindric grid with an angular step of 1 degree both in latitude and longitude. For a given polarization, X or Y, the weight is the reciprocal of the radiometric noise variance. Finally, a four-point smoothing is applied to the data. In Figure 1 we show the two L3 maps. Notice that a large area close to the coast has been discarded following a criterion based on the land-sea mask interpolated into the antenna frame for each snapshot.

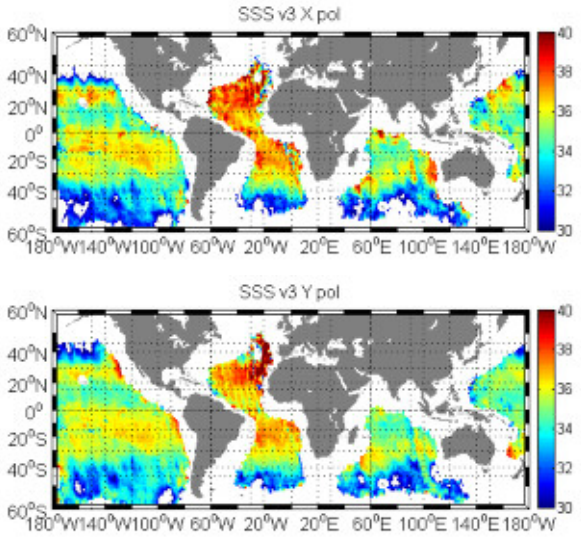

Fig. 1. SSS as derived from T_X (top) and T_y (bottom).

3. COMPARISON WITH CLIMATOLOGY

In a first validation, the retrieved SSS is compared against WOA 2005 [3] (monthly March climatology), which is derived from the World Ocean Database. Figure 2 shows the map of the difference between Levitus climatology and the two SMOS L3 maps.

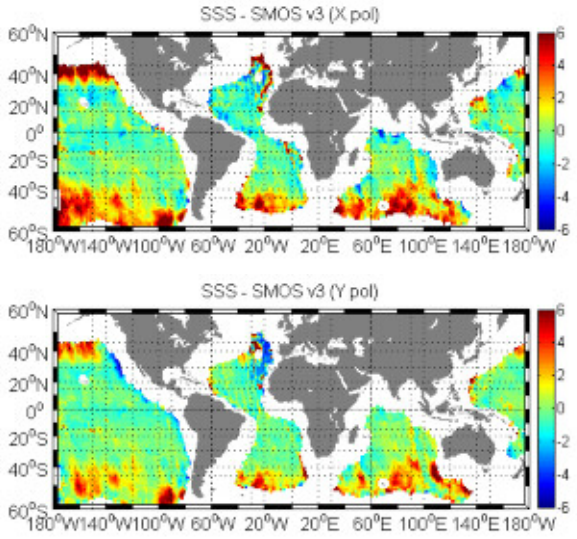

Fig. 2. Differences between SSS as derived from T_X (top) and T_y (bottom) with respect to Levitus climatology.

As evidenced in the figure, differences between Levitus climatology and SMOS are small at low latitudes. The largest differences, at high latitudes, are attributed to both the inadequate representation of wind in the geophysical model, and to the lower sensitivity of T_B to SSS. In Figure 3 we present a statistical analysis of the differences. The observed biases (averages of the differences) could be explained with the particular salinity anomalies in this particular year; however, the standard deviation (well above 1 psu) is rather large, taking into account the expected variability of salinity anomalies. This issue will be discussed further in the next Section when SMOS SSS maps are compared to in situ measurements

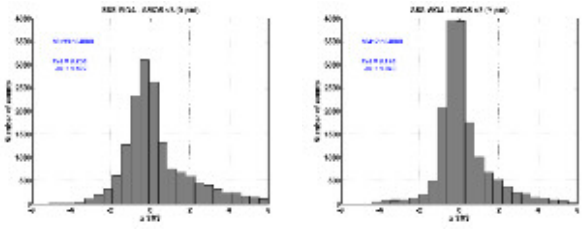

Fig. 3. Histograms of the SSS differences with respect to Levitus climatology. Left: differences for SSS derived from T_X; Right: differences for SSS derived from T_Y.

4. COMPARISON WITH ARGO

A match-up database being built at BEC is used to compare the reconstructed SSS field against the uppermost value of salinity from Argo. A total of 1438 profiles are found for the period 2010/03/10 to 2010/03/15 (meeting the double criteria of having salinity data and an uppermost measure not deeper than 10 m). The original ARGO dataset that fed our database was downloaded from Coriolis GDAC ftp facility. Some profiles were disregarded according to the information present in the "Argo grey list" (http://www.usgodae.org/pub/outgoing/argo/ar_greylist.txt), reducing the number of valid profiles to 1060 data. In Figure 4 we present a map of the differences between ARGO measurements and SMOS L3 maps.

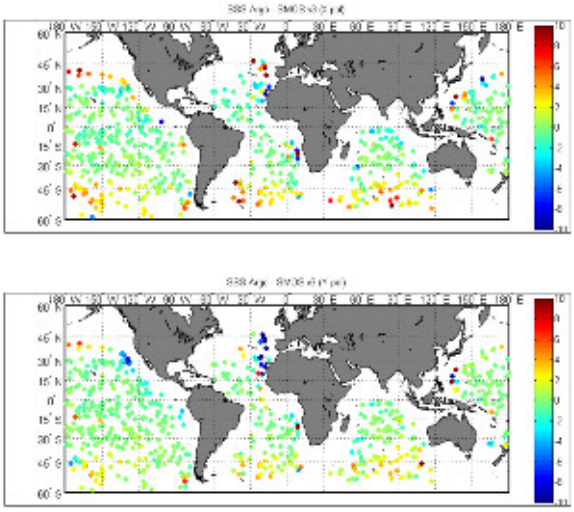

Fig. 4. Differences between SSS as derived from T_X (top) and T_y (bottom) with respect to Argo floats.

Differences with Argo data have a spatial structure similar to the differences against WOA-derived Levitus climatology. We have also computed the histograms for the differences, as shown in Figure 5. The tails in the X-pol histogram are heavier than those of Y-pol histogram, and both exhibit a clear positive skewness. Such high positive tail is associated to high latitude range with systematic higher wind and roughness conditions which impact is likely erroneously quantified by the pre-launch forward models. The standard deviation is even greater than that observed when the data was compared to Levitus climatology, which was expected because of the differences of sampling scales. Even assuming that the observed variability is completely random and uncorrelated, this would lead to L3 maps for a one-month period with a minimum uncertainty of 0.6 psu, well above of the 0.1 psu defined as the mission objective. It is hence evident that data quality must be significantly improved in the previous stages of the processing, probably both at the image reconstruction and SSS inversion levels.

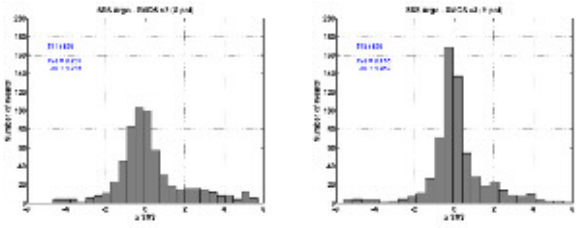

Fig. 5. Histograms of the SSS differences with respect to Argo floats. Left: differences for SSS derived from T_X; Right: differences for SSS derived from T_Y.

5. SINGULARITY ANALYSIS

Novel analytic tools issued from the theory of turbulence have revealed, when applied to satellite data, the existence of scale-invariant properties of oceanic tracer fields as the SSS[4, 5, 6]. Here, the Microcanonical Multifractal Formalism[7] has been used to assess the realism of the dynamical features present in SMOS L3 maps.

In Figure 6 we present maps of singularity exponents associated to different L3 maps. The singularity exponent of a point is a dimensionless measure of the regularity degree of the scalar at that given point [7]. These differences of behaviour are thought to be in correspondence to the differences in shear of the underlying flow; in fact, some recent works evidence that there is a relation between singularity maps and surface streamlines, independently of the parameter being analyzed (e.g., temperature, salinity, or chlorophyll concentrations) [8]. In the maps shown in Figure 6 we have depicted the most irregular behaviours (i.e., most singular exponents) with the brightest color, while the most regular points are shown with the darkest colors. In the Figure, we present the singularity exponents of the SSS from X- and Y- pol, together with the singularity exponents of the averaged SST for the same period. The singularity map of SST clearly reveals the patterns of the global oceanic circulation, while those of the SSS maps are more strongly affected by contamination. Even so, there are clearly recognizable geophysical features in the eastern tropical Pacific Ocean which SSS maps display, features also present in the SST singularity map. More interestingly, this technique reveals clearly the actual extent of the combined effects of RFI and land interferences, which far exceed the coastal strip we first removed; as an example, in the case of T_y, some coherent interference lines can be observed all over the Northern Equatorial Atlantic, suggesting a clear contribution of non-geophysical processes.

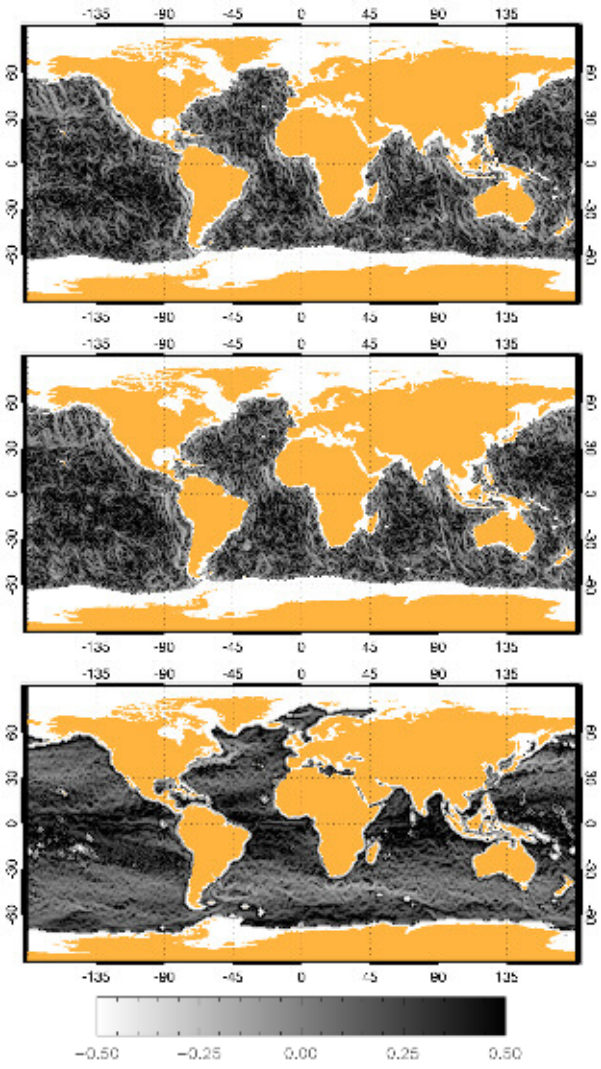

Fig. 6. SSS as derived from T_X (top) and T_y (bottom) with respect to Argo floats.

6. CONCLUSIONS

The results indicate that current 6-day gridded SSS products are not between the mission accuracy goals, specially outside tropical regions.

Large error variance is observed both at Y-pol and even larger at X-pol. First order error reduction is expected in the near-future from a consistent adjustment of forward models and bias correction procedures. Further, image reconstruction needs to be refined as well as SSS retrieval algorithm.

The singularity analysis of the retrievals illustrate the actual extent of RFI and land interferences that, as in the case of the equatorial Atlantic Ocean, may spread from coast to coast.

Acknowledgements

The authors are grateful to J. Tenerelli for providing access to his analysis software. CP34 and SMOS-BEC development has been funded by the Spanish Ministry of Education and Science through research grants ESP2002-11604-E, ESP2004-00671, ESP2005-06823-C05-01 and ESP2007-65667-C04.

7. REFERENCES

[1] Y.H. Kerr, P. Waldteufel, J.P. Wigneron, F. Cabot, J. Boutin, M.J. Escorihuela, J. Font, N. Reul, C. Gruhier, S. Juglea, S. Delwart, M. Drinkwater, A. Hahne, and M. Martín-Neira, "The Challenging Sea Surface Salinity Measurement from Space," Proceedings of IEEE, 98(5): 666-681, doi: 10.1109/JPROC.2009.2033096, 2010.

[2] J. Font, A. Camps, and J. Ballabrera, "Microwave aperture synthesis radiometry: Setting the path for operational sea salinity measurement from space," *Remote Sensing of European Seas* (Chapter 16), V. Barale, M. Gade eds., Springer-Verlag, pp 223-238. ISBM: 978-1-4929-6771-6, 2008.

[3] J.I. Antonov, R.A. Locarnini, T.P. Boyer, A.V. Mishonov, and H.E. Garcia, "World Ocean Atlas 2005, Volume 2: Salinity," S. Levitus ed., NOAA Atlas NESDIS 62, U.S. Government Printing Office, Washington, D.C. 182 pp., 2006.

[4] J. Isern-Fontanet, A. Turiel, E. Garcia-Ladona, and J. Font, "Microcanonical multifractal formalism: application to the estimation of ocean surface velocities," *Journal of Geophysical Research*, vol. 112, pp. C05024, 2007.

[5] V. Nieves, C. Llebot, A. Turiel, J. Solé, E. García-Ladona, M. Estrada, and D. Blasco, "Common turbulent signature in sea surface temperature and chlorophyll maps," *Geophysical Research Letters*, vol. 34, pp. L23602, 2007.

[6] A. Turiel, J. Solé, V. Nieves, J. Ballabrera-Poy, and E. García-Ladona, "Tracking oceanic currents by singularity analysis of micro-wave sea surface temperature images," *Remote Sensing of Environment*, vol. 112, pp. 2246–2260, 2008.

[7] A. Turiel, H. Yahia, and C. Pérez-Vicente, "Microcanonical multifractal formalism: a geometrical approach to multifractal systems. Part I: Singularity analysis," *Journal of Physics A*, vol. 41, pp. 015501, 2008.

[8] A. Turiel, V. Nieves, E. García-Ladona, J. Font, M.-H. Rio, and G. Larnicol, "The multifractal structure of satellite temperature images can be used to obtain global maps of ocean currents," *Ocean Science*, vol. 5, pp. 447–460, 2009.